American Journal of Pathology, Vol. 168, No. 6, June 2006

DOI: 10.2353/ajpath.2006.051113

Immunopathology and Infectious Diseases

Multiorgan Autoimmune Inflammation, Enhanced Lymphoproliferation, and Impaired Homeostasis of Reactive Oxygen Species in Mice Lacking the Antioxidant-Activated Transcription Factor *Nrf2*

Qiang Ma,* Lori Battelli,† and Ann F. Hubbs†

From the Receptor Biology Laboratory, Toxicology and Molecular Biology Branch, and the Experimental Pathology Laboratory,† Pathology and Physiology Research Branch, Health Effects Laboratory Division, National Institute for Occupational Safety and Health, Centers for Disease Control and Prevention, Morgantown, West Virginia*

Nuclear factor erythroid 2-related factor 2 (Nrf2) is an antioxidant-activated cap "n" collar basic leucine zipper transcription factor. To assess the function of Nrf2 in the antioxidant response, we examined mice with targeted disruption of the *Nrf2* gene. Nrf2-null mice developed complex disease manifestations, with a majority exhibiting a lupus-like autoimmune syndrome characterized by multiorgan inflammatory lesions with a marked female predominance, appearance of anti-double-stranded DNA antibodies in young adulthood, intravascular deposition of immunoglobulin complexes in blood vessels, and premature death due to rapidly progressing membranoproliferative glomerular nephritis. Mechanistic analyses revealed that the null mice showed enhanced proliferative response of $CD4^+$ T cells, altered ratios of $CD4^+$ and $CD8^+$ cells, and increased oxidative lesions in tissues. Analyses of antioxidant-induced gene expression showed that the knockout mice were devoid of the basal and inducible expression of certain phase 2 detoxification enzymes and antioxidant genes in hepatic and lymphoid cells *in vivo*. Our findings suggest that Nrf2 mediates important antioxidant functions involved in the control of peripheral lymphocyte homeostasis and autoimmune surveillance. ***(Am J Pathol 2006, 168:1960–1974; DOI: 10.2353/ajpath.2006.051113)***

The nuclear factor erythroid 2 (NF-E2)-related factor 2 (Nrf2) belongs to a subfamily of the basic leucine zipper transcription factors termed CNC bZip for cap "n" collar basic leucine zipper. The CNC bZip proteins are characterized by a highly conserved 43-amino acid module localized immediately N-terminal to the bZip DNA-binding region. The module is homologous in sequence to a region in the CNC gene, a homeotic gene involved in cephalic patterning during embryogenesis of *Drosophila*,[1,2] hence the name CNC (for cap "n" collar). The CNC bZip family includes NF-E2, Nrf1, Nrf2, Nrf3, Bach1, and Bach2.[3–8] NF-E2, the founder member of the group, controls the transcriptional regulation at the hypersensitive site 2 of the human β-globin gene cluster locus.[6] Nrf1, Nrf2, and Nrf3 were cloned as a result of searching for NF-E2-related proteins binding to the NF-E2 DNA-binding sequence, whereas Bach1 and Bach2 were proteins distantly related to NF-E2 but capable of binding to MafK,[8] a member of the small Maf proteins that form heterodimers with the CNC bZip proteins for DNA binding.

Whereas NF-E2 is strictly expressed in hematopoitic cells and is required for regulation of β-globin gene expression, Nrf2 is ubiquitously expressed in animal tissues, and its role in β-globin expression remains uncertain.[9] Instead, increasing evidence reveals that Nrf2 mediates the antioxidant response element (ARE)-dependent transcriptional regulation of a battery of genes. These include phase II enzymes such as NAD(P)H:quinine oxidoreductase 1 (NQO1) and glutathione *S*-transferase A1 (GSTA1), which detoxify endogenous and exogenous chemicals through reduction and conjugation reactions, and antioxidative enzymes and proteins such as thioredoxin, heme oxy-

Accepted for publication March 13, 2006.

The findings and conclusions in this report are those of the authors and do not necessarily represent the views of the National Institute of Occupational Safety and Health.

Address reprint requests to Qiang Ma, Receptor Biology Laboratory, Toxicology and Molecular Biology Branch/Health Effects Laboratory Division/National Institute for Occupational Safety and Health/Centers for Disease Control and Prevention, Mailstop 3014, 1095 Willowdale Rd., Morgantown, WV 26505. E-mail: qam1@cdc.gov.

genase 1 (HO-1), and ferritin, which participate in reactive oxygen species (ROS) metabolism or directly scavenge ROS. Thus, Nrf2 appears to function as a key regulator of the antioxidant response. Consistent with this notion, a number of genetic studies have implicated Nrf2 in a range of protective responses against chemical-induced lesions or disease states. Loss of function of Nrf2 is associated with increased sensitivity to chemical carcinogenesis such as benzo(a)pyrene-induced gastric neoplasia,[10] acetaminophen-induced hepatotoxicity,[11] hyperoxic lung damage,[12] pulmonary injury by butylated hydroxytoluene[13] or diesel exhaust,[14] and premature ovarian failure by the occupational ovotoxicant 4-vinyl cyclohexine diepoxide.[15] Although Nrf2 is dispensable for life in mice, it cooperates with Nrf1 to regulate antioxidant gene expression during early embryonic development. A combined deletion of Nrf1 and Nrf2 results in marked oxidative stress and increased apoptosis in the liver leading to embryonic lethality, suggesting overlapping functions among the CNC bZip proteins and possibly compensation for each other in the defense against oxidative stress during embryonic hepatogenesis.[16]

The molecular mechanism of Nrf2 action is best understood for the induction of phase II genes, such as the induction of *Nqo1* by phenolic antoxidants.[17,18] In the absence of an activator, Nrf2 is a labile protein localized in the cytoplasm forming a complex with Keap1. Keap1 anchors Nrf2 in the cytoplasm by interacting with cytoskeletal proteins. Moreover, Keap1 regulates the ubiquitin-26S proteasome-mediated turnover of Nrf2 through a Cul3-based E3 ligase. Binding of tert-butylhydroquinone (tBHQ) to Keap1 stabilizes Nrf2. Activated Nrf2 translocates into the nucleus and forms a heterodimer with a Maf protein. The dimer then binds to AREs located in the enhancer regions and mediates the transcription of the genes. Variations of this Nrf2/ARE paradigm have been observed in the transcriptional regulation of a number of genes, suggesting high adaptability of Nrf2 action in a broad range of biological functions. For instance, Nrf2 can interact with activating transcription factor 4 in the induction of *Ho-1*,[19] compete with Jun/Fos for binding to ARE/AP1 sites in the induction of thioredoxin by hemin,[20] or cross-interact with aryl hydrocarbon receptor (AhR) signaling for induction of murine *Nqo1* by AhR agonist 2,3,7,8,-tetrachlorodibenzo-*p*-dioxin (TCDD).[18]

Here, we report that loss of Nrf2 in mice is associated with the development of autoimmune-mediated lesions in multiple tissues. The lesions were characterized by disseminated inflammation, appearance of anti-double-stranded DNA (dsDNA) antibodies at young ages, vascular deposition of immunoglobulin complexes, and premature death due primarily to rapidly progressing glomerulonephritis. Surviving mice frequently died of neoplasia of lymphoid, histiocytic, or endothelial origins. Nrf2-null mice exhibited increased proliferative response of $CD4^+$ cells and altered ratios of $CD4^+$ and $CD8^+$ peripheral T cells. Finally, the Nrf2-null mice were devoid of the basal and inducible expression of a number of phase II and antioxidant-responsive genes and concomitantly displayed increased oxidative lesions in multiple tissues. Together, the findings suggest interplay between Nrf2 function, ROS defense, and autoimmune surveillance in the development of autoimmune disorders.

Materials and Methods

Mice

Nrf2 knockout mice (kindly provided by Dr. Y.W. Kan, University of California, San Francisco, CA) were re-derived at Jackson Laboratory to assure specific pathogen-free status.[18] *Nrf2*$^{-/-}$ and *Nrf2*$^{+/+}$ mice on a genetic background of 129SVJ were maintained at an environmentally controlled National Institute for Occupational Safety and Health animal facility, which is fully accredited by the Association for Assessment and Accreditation of Laboratory Animal Care International. The mice were barrier maintained with a light/dark cycle of 12 hours at a constant temperature (22°C) in HEPA-filtered, individually ventilated microisolator cages (Thoren Caging Systems, Hazleton, PA). Irradiated food (6% fat; 7913; Harlan-Teklad, Madison, WI) and water were provided *ad libitum*. Bedding was sterile Beta chip from Northeastern Products Company (Warrensburg, NY). Mice were observed daily for signs of illness. Moribund mice showing severe edema or lethargy were sacrificed for histopathological examinations. Mouse breeding, morbidity, and mortality were recorded using the Colony software, version 3.0 (Locus Technology, Inc., Orland, ME).

Isolation of Peripheral Lymphocytes and Flow Cytometry Analysis

Lymph nodes (from the mandibular and axillary regions) and spleen were collected. Lymphocytes were isolated by gentle disruption of the tissues with the flat end of a syringe plunger against the bottom of a 70-μm nylon cell strainer (Becton Dickinson Labware, Franklin Lakes, NJ), followed by centrifugation at 1200 $\times$ *g* for 10 minutes. Red blood cells in spleen samples were removed by lysis with ammonium chloride lysing reagent (BD Pharmingen, San Diego, CA) and repeated centrifugation and washing. $CD4^+$, $CD8^+$, or $CD45R/B220^+$ cells were isolated using BD IMagnet according to manufacturer's instructions (BD Pharmingen). Briefly, an appropriate number of lymph node cells or splenocytes were suspended in 1$\times$ BD IMag buffer and blocked for nonspecific binding with anti-mouse CD16/CD32 monoclonal antibody (BD Pharmingen) on ice for 15 minutes, followed by a brief spin. Cell pellets were re-suspended in 0.5 ml of IMag buffer, mixed with 50 μl of BD IMag anti-mouse CD4, CD8a, or CD45R/B220 particles, and incubated at 4°C for 30 minutes. The cells labeled with IMag particles were placed in the BD IMagnet and were separated from unlabeled cells by magnetic force. The separation process was repeated one more time. Isolated $CD4^+$, $CD8^+$, or $CD45R/B220^+$ cells were examined for purity by fluorescence-acitvated cell sorter (FACS) as described below and were used for cell proliferation and FACS analysis.

For staining of cell surface antigens, ~5×10^5 to 1×10^6 cells were blocked with anti-mouse CD16/CD32 on ice for 15 minutes. The cells were then stained with R-phycoerythrin-conjugated anti-mouse CD4, flourescein isothiocyanate (FITC)-conjugated anti-mouse CD8a, or peridinin chlorophyll-α protein-conjugated anti-mouse CD45R/B220 monoclonal antibodies (BD Pharmingen) on ice in the dark for 15 minutes. After washing, the cells were resuspended in staining buffer and analyzed using FACSCalibur (Becton Dickinson, San Jose, CA).

Lymphocyte Proliferation Assay

To analyze responses of lymphocytes to proliferative stimuli, splenocytes, lymph node cells, or isolated $CD4^+$, $CD8^+$, and $CD45R/B220^+$ cells were cultured in RPMI 1640 (Invitrogen, Carlsbad, CA) supplemented with 4 mmol/L glutamine and 10% fetal bovine serum. To measure response to anti-CD3, cells (5×10^4 or 1×10^5) were seeded in a 96-well BD BioCoat T-Cell Activation Plate precoated with anti-CD3 antibodies (BD Discovery Labware, San Diego, CA) and incubated at 37°C with 5% CO_2 for 48 hours. Proliferation of the cells was measured using the 3-(4,5-dimethyl thiazole-2-yl)-2,5-diphenyl tetrazolium bromid (MTT) kit from Roche Applied Science (Indianapolis, IN). MTT labeling reagent (10 μl) was added to each well, and the plate was incubated for 4 hours in a CO_2 incubator, followed by adding 100 μl of a solubilization solution into each well. The plate was kept overnight in the incubator, and cell proliferation was measured at 550 nm using a plate reader (Spectra Max 340PC; Molecular Devices, Sunnyvale, CA). For B-cell proliferation assay, purified B cells were activated with goat $F(ab')_2$ anti-mouse IgM (Jackson ImmunoResearch, West Grove, PA) or lipopolysaccharide (20 μg/ml; Sigma, St. Louis, MO) for 48 hours. Proliferation was measured with the MTT kit as described above.

Antibody Titration

Blood samples were collected from tail veins of age-matched (5- to 7-month-old) male and female $Nrf2^{+/+}$, $Nrf2^{+/-}$, or $Nrf2^{-/-}$ mice (all in the 129SVJ background) and C57BL/6J mice (as a separate control; The Jackson Laboratories, Bar Harbor, ME) into serum tubes (Becton Dickinson). Sera were prepared and measured for mouse anti-dsDNA or anti-single-stranded DNA antibodies using enzyme-linked immunosorbent assay (ELISA) kits from Alpha Diagnostic International (San Antonio, TX) according to supplier's instructions. ELISA was measured at 450 nm using Spectra Max 340PC plate reader.

Determination of Blood Urea Nitrogen (BUN), Total Protein, and Hematocrit

Serum BUN and total protein were determined using a COBAS MIRA Plus Chemistry Analyzer (Roche Diagnostics Corp., Indianapolis, IN). Blood was collected from the abdominal vena cava, placed in a serum microtainer tube, and incubated for approximately 20 minutes. Blood was centrifuged for 15 minutes at 3000 rpm, and serum was collected and placed in a vial. The vial was then placed in the Chemistry Analyzer. BUN and total protein were determined using Reagent for BUN from Roche Diagnostics or Reagent for Total Protein from Sigma, respectively. For hematocrit determination, blood was drawn from the abdominal vena cava into standard heparinized hematocrit tubes. One end of each tube was sealed with clay tube sealer. The tubes were centrifuged on a Damon IEC MB centrifuge (Damon, Needham Heights, MA) at 13,700 $\times$ *g* for 5 minutes. Hematocrit was determined with a Damon microcapillary reader (Damon).

Measurement of Lipid Peroxidation

Free malondialdehyde (MDA) was measured using the Bioxytech MDA-586 kit from OxisResearch (Portland, OR). Briefly, kidney, liver, and heart tissues were collected from female $Nrf2^{-/-}$ or $Nrf2^{+/+}$ mice at 6 months of ages or as indicated in figures. The tissues were homogenized in the presence of 5 mmol/L butylated hydroxytoluene. Extracts were prepared by centrifugation at 10,000 $\times$ *g* for 10 minutes. MDA contents were assayed and measured spectrophotometrically according to instructions provided by the manufacturer.

Treatment of Mice and Analysis of mRNA Expression

$Nrf2^{+/+}$ and $Nrf2^{-/-}$ mice (2 months old) were treated with corn oil or 3-t-butyl-4-hydroxy anisol (BHA). BHA is administered by gavage on days 1 and 3 at a dose of 400 mg/kg body weight. Liver and spleen samples were collected on day 4 after BHA treatment and were stored in RNALater (Qiagen, Valencia, CA). Total RNA was prepared using a Qiagen Total RNA isolation kit (Qiagen). Northern blotting was performed as follows. RNA samples (5 μg) were fractionated in a 1% agarose-formaldehyde gel and transferred to a Nytran membrane. The blot was probed with a dioxigenin (DIG)-labeled riboprobe prepared with the DIG-labeling kit (Roche Applied Science) for mouse genes according to established procedures.[21] Signals were visualized by chemiluminescence using a DIG RNA detection kit with CDP Star as a substrate (Roche Applied Science). Parallel blots of the same samples were probed with a DIG-labeled mouse actin probe to ensure equal loading. Results shown were repeated two times in separate experiments with consistent observations.

Real-time polymerase chain reaction (PCR) was performed using SYBR Green PCR master mix (Applied Biosystems, Foster City, CA) on a Bio-Rad iCycler (Bio-Rad, Hercules, CA) following standard procedures. Briefly, single-stranded cDNA was synthesized from 1 μg of total RNA using Superscript III reverse transcriptase (Invitrogen). For PCR reach reaction, 2 μl of DNA template, 2 μl of forward and reverse primers (10 μmol/L each), 25 μl of SYBR Green PCR Master Mix, and 19 μl of

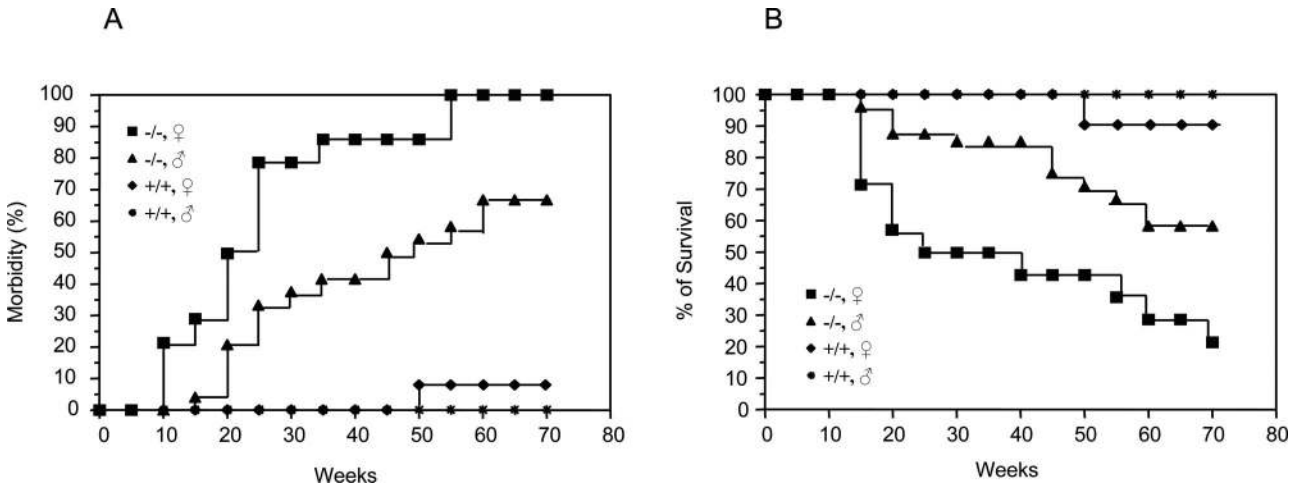

Figure 1. Spontaneous morbidity and mortality of Nrf2 knockout mice. Female and male Nrf2 knockout mice (*Nrf2*$^{-/-}$) and wild-type control mice (*Nrf2*$^{+/+}$) were individually barrier-maintained in an environmentally controlled facility. Morbidity and mortality were examined and recorded daily. **A:** Morbidity. **B:** Survival over time. Genotype and gender are indicated. *x* axis indicates the ages of the mice in weeks. Animals in the study: wild type, 10 male and 10 female; *Nrf2*$^{-/-}$, 24 male and 14 female. Morbidity reflects a broad range of signs of illness as described in Results. Survival is based on spontaneous deaths and euthanasia of moribund mice.

water were added to a final volume of 50 μl. Thermal cycling was performed as follows: 95°C for 3 minutes as initial denaturing, followed by 45 cycles of 94°C for 30 seconds, 60°C for 30 seconds, and 72°C for 60 seconds, and a final extension at 72°C for 2 minutes. Threshold cycles (C_T values) were determined using the iCycler IQ software (Bio-Rad). Real-time PCR results were normalized using 1% of input as an internal control. Relative DNA amounts were calculated from the C_T values for each sample by interpolating into the standard curve obtained using a series dilution of standard DNA samples run under the same conditions. Primer sets used for real-time PCR were as follows: NQO1 forward, 5′-AACGGGAAGATGTGGAGATG-3′, and reverse, 5′-CGCAGTAGATGCCAGTCAAA-3′; HO-1 forward, 5′-GAGCAGAACCAGCCTGAACTA-3′, and reverse, 5′-GGTACAAGGAAGCCATCACCA-3′; and β-actin forward, 5′-GACCTCTATGCCAACACAGT-3′, and reverse, 5′-ACTCATCGTACTCCTGGTG-3′.

Histological, Immunofluorescent, and Electron Microscopy

Tissue samples were fixed in 10% neutral buffered formalin for 1 day, subsequently routinely processed, and embedded in paraffin. Sections of 5 μm thickness were stained with hematoxylin and eosin (H&E) or with PAS. Slides were interpreted by a board-certified veterinary pathologist blinded to the genotypes of individual animals. For immunofluorescent studies of immunoglobulin complex deposition, fresh kidneys or other tissues were flash frozen in liquid nitrogen and subsequently stored at −80°C. Frozen sections were prepared using a cryostat. Sections were washed with phosphate-buffered saline (PBS; Sigma) three times (10 minutes each), followed by a 5-minute wash with PBS. Nonspecific binding was blocked by sequential 10-minute baths in 5% PBS/bovine serum albumin (IgG free) and 5% pig serum (Biogenex, San Ramon, CA). Primary antibodies were incubated with tissue sections for 2 hours in the dark as follows: FITC-goat anti-mouse IgG+A+M (Zymed, South San Francisco, CA) 1:20 in PBS plus 10% goat serum; Alexa Fluor 488-goat anti-mouse IgG (Molecular Probes, Eugene, OR) 1:20 in PBS; Alexa Fluor 488-goat anti-mouse IgM (Molecular Probes) 1:20 in PBS; or fluorescein-conjugated goat IgG fraction against mouse complement C3 (ICN/Cappell, Aurora, OH) 1:400 in PBS. Sections were rinsed three times with PBS (each for 5 minutes), covered with coverslips in Gelmount (Biomeda, Foster City, CA), and examined under a fluorescent microscope. For transmission electron microscopy, fresh kidney samples were preserved in Karnovsky's fixative, postfixed in osmium tetroxide, mordanted in tannic acid, and stained *en bloc* in uranyl acetate. The tissues were then dehydrated in alcohol and embedded in Epon. The sections were stained with uranyl acetate and lead citrate. Kidney samples were examined ultrastructurally using a JEOL 1220 electron microscope.

Results

Spontaneous and Gender-Dependent Morbidity and Mortality

The Nrf2-null mice bred normally, and their offspring grew and matured similarly to *Nrf2*$^{+/+}$ mice. However, the mice developed a range of signs of illness after 2 months of age (Figures 1 and 2). Manifestations of illness were diverse, including reduced body weight, subcutaneous edema, which often started at the facial area and spread to the whole body gradually (Figure 2A), pale ears and toes, cutaneous ulcers, ring-shaped tail redness and necrosis (Figure 2B), eye inflammation (Figure 2A), and neurological symptoms (dysmetria, tremors, lethargy, and seizures) (Figure 2A). These signs were rarely ob-

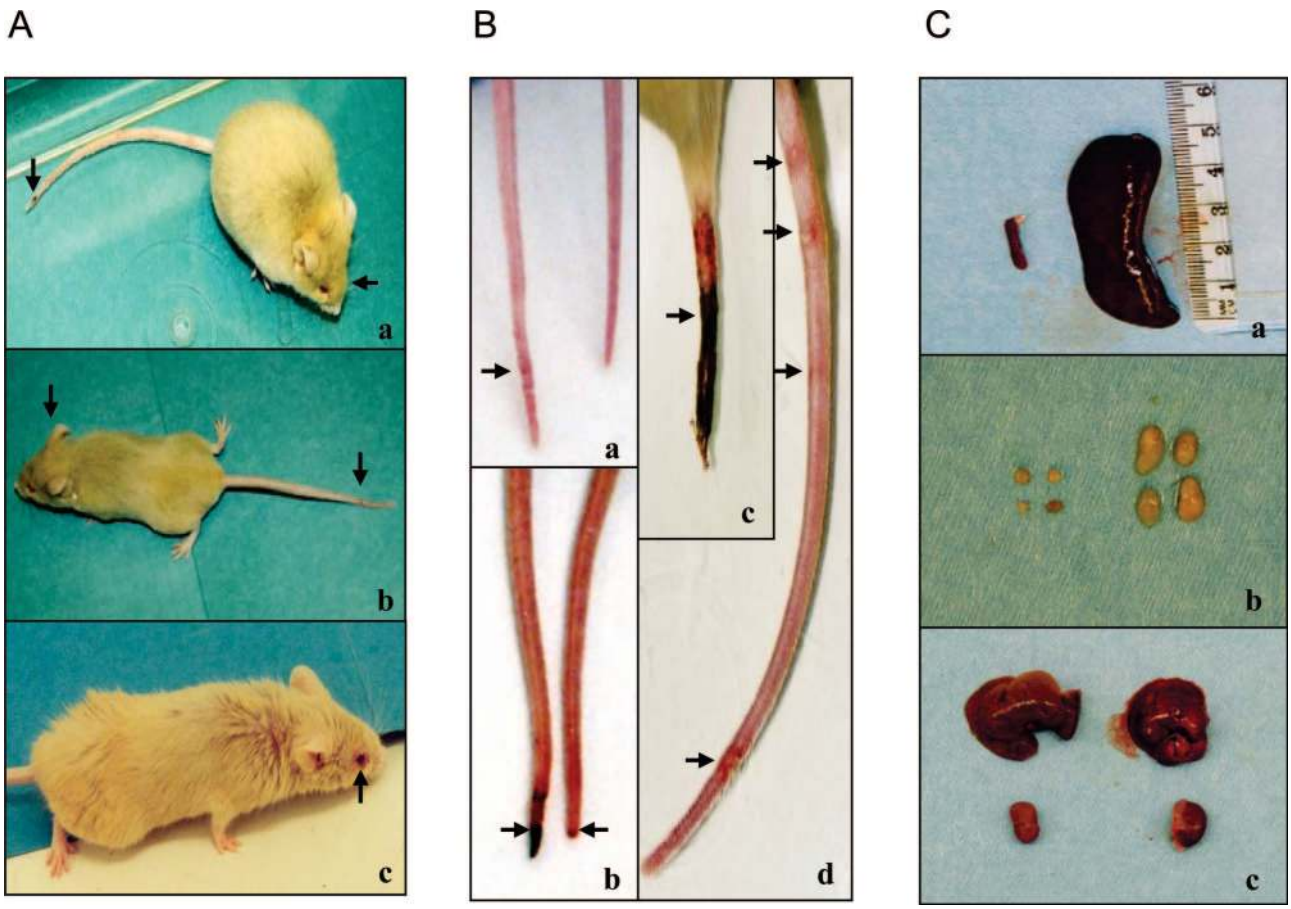

Figure 2. Gross phenotypes of Nrf2-null mice. **A:** *Nrf2*$^{-/-}$ mice exhibited diverse signs of illness, including facial and whole-body edema, tail necrosis (**a** and **b**, indicated by **arrow**), dysmetria (**b**), and conjunctivitis (**c**). **B:** Tails of Nrf2-null mice developed focal, multifocal, or circumferential erythematous lesions (**a**–**d**); initial tail lesions are at the distal end and progress proximally (**b** and **c**). **C:** Splenomegaly and enlarged lymph nodes. Splenomegaly (**a**) and enlarged lymph nodes (**b**) were seen in *Nrf2*$^{-/-}$ (**right**) but not *Nrf2*$^{+/+}$ (**left**) genotypes. The sizes of the liver and kidney were similar from the same mice (**c**).

served in *Nrf2*$^{+/+}$ mice with the same genetic background during the period of study (Figure 1A). Moreover, a clear female predominance of the illness was seen (Figure 1A). The morbidities of the female mice were 29, 79, and 100% at ages of 15, 25, and 55 weeks, respectively, whereas, those of the male were 4, 33.3, and 58.3% at the same ages (Figure 1A). In addition, female mice appeared to develop signs of illness earlier (10 versus 14 weeks) and more severely than their male littermates.

The Nrf2-null mice exhibited shortened life spans compared with the wild-type control mice (Figure 1B). Similar to the morbidity, a clear gender-dependent difference in survival was observed. Female mice died earlier and at a higher rate than male mice. The survival rates of the female at ages of 15, 25, and 55 weeks were 71.4, 50, and 21.4%, respectively, substantially lower that those of the male (ie, 96, 87.5, and 58.3% at the same ages). Thus, loss of Nrf2 in mice caused a spontaneous, gender-dependent, and diverse spectrum of disease manifestations and mortality in the absence of apparent exposure to exogenous toxic chemicals.

Glomerulonephritis

Histopathological examination of the diseased mice revealed a high prevalence of glomerulonephritis. Among the mice that died or were euthanized because of severe illness, the glomerulonephritis prevalence was 88% (31 with glomerulonephritis, 3 without glomerulonephritis, and 1 unevaluated because of extensive tissue autolysis). The mean age of Nrf2-null mice with glomerulonephritis was 9 ± 1 (SE) months with a range of 2 to 22 months. Glomerulonephritis was the primary cause of death in 69% (22 of 32) of Nrf2-null mice in this necropsy series, causing death in mice as young as 2 months of age. Glomerulonephritis was seen in both female and male mice and was the cause of death in 88% (15 of 17) of female and 47% (7 of 15) of male mice. Spontaneous death was often accompanied by subcutaneous edema and lethargy. The corresponding histopathological alterations seen in affected Nrf2-null mice were varying manifestations of membranoproliferative glomerulonephritis (Figure 3). Antemortem BUN concentration was elevated in mice with the most severe histopathological changes in glomeruli (Figure 4). In wild-type and heterozygous mice,

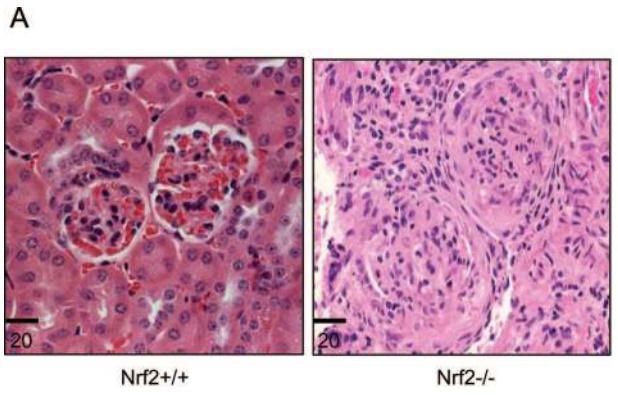

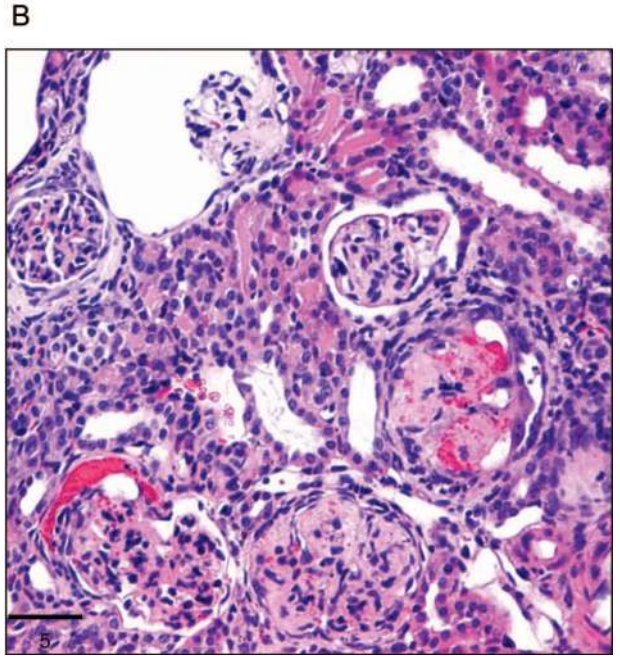

Figure 3. Glomerulonephritis in Nrf2-null mice. Kidneys from *Nrf2*$^{-/-}$ and age-matched *Nrf2*$^{+/+}$ mice were sectioned and stained with hematoxylin and eosin. **A:** Glomeruli from control mice showing two normal glomeruli and surrounding tubules (**left**) and glomerulonephritis from Nrf2-null mice with subcutaneous edema (**right**). The glomeruli show diffusive, membranoproliferative glomerulonephritis with enlarged glomeruli, proliferation of mesangial and parietal epithelial cells, glomerulosclerosis, and loss of Bowman's space and capillary lumen. **B:** A kidney section from a *Nrf2*$^{-/-}$ mouse showing acute and chronic glomerulonephritis consistent with multiple inflammatory episodes: a relatively normal glomerulus; acute glomerulonephritis with bleeding into the Bowman's space; chronic lesions with necrosis, closure of Bowman's space and capillary lumen, and thickening of Bowman capsule; and, a glomerulus with enlarged Bowman's space and atrophy of glomerular capillary loops. Bars are in microns.

membranoproliferative glomerulohephritis was uncommon, and signs of renal failure were not observed.

In most cases of glomerulonephritis, glomeruli were enlarged with mesangial cell proliferation, thickening of glomerular basement membranes, and frequent adhesions between Bowman's capsule and glomeruli. Variable fibrosis indicated chronicity, ranging from fibrosis of Bowman's capsule to complete glomerulosclerosis. In many kidneys, renal tubules and Bowman's space contained eosinophilic material consistent with proteinuria. In the most severely affected null mice, both acute and chronic glomerulonephritis were manifested by varying

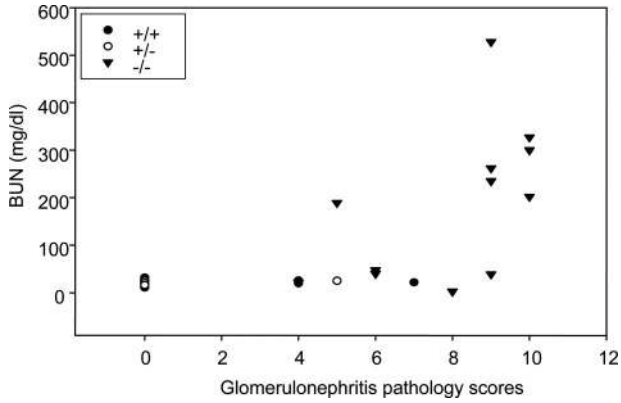

Figure 4. Correlation of BUN and glomerulonephritis severity. Antimortem blood urea contents (BUN) and glomerulonephritis pathology scores (reflecting severity of glomerulonephritis) of *Nrf2*$^{+/+}$, *Nrf2*$^{+/-}$, and *Nrf2*$^{-/-}$ mice were evaluated for correlation using the Sigma Plot software.

degrees of cellular proliferation, necrosis, bleeding into Bowman's space, obliteration of Bowman's space, and complete glomerulosclerosis (Figure 3B). The severity of the kidney lesions often correlated with age and morbidity. In older mice and those with signs of renal disease, fibrosis of glomeruli was observed; whereas in younger mice and those with milder signs of disease, focal and lobular glomerular changes were common.

Immunofluorescent staining revealed the deposition of large immunoglobulin complexes in the glomeruli of *Nrf2*$^{-/-}$ compared with much smaller or no complexes in *Nrf2*$^{+/+}$ mice (Figure 5, compare a and b); the immunoglobulines detected in the complexes included IgG (Figure 5), IgA, and IgM (data not shown). Similarly, deposition of complement C3 in glomeruli was markedly

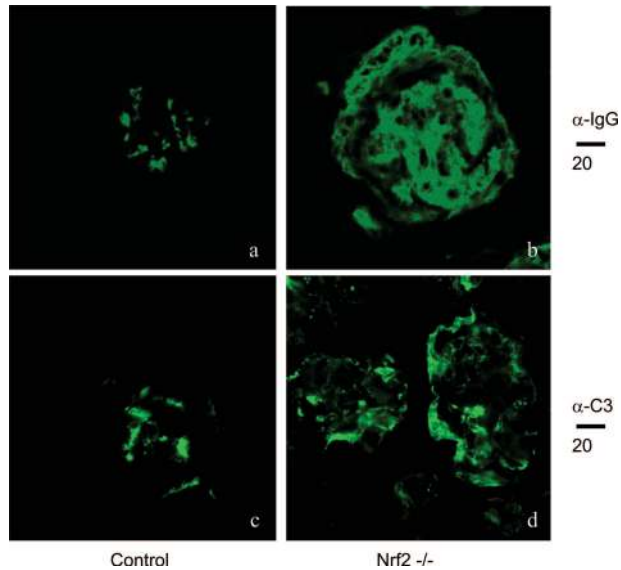

Figure 5. Immunostaining of immunocomplex deposition in glomeruli. Kidneys from *Nrf2*$^{+/+}$ (age-matched control, **a** and **c**) and *Nrf2*$^{-/-}$ (**b** and **d**) mice were sectioned and processed for immunofluorescent staining with anti-IgG (α-IgG, **a** and **b**) or anti-complement C3 (α-C3, **c** and **d**) antibodies followed by FITC-conjugated secondary antibodies, as described in Materials and Methods. Fluorescent microscopy showed 1) a large amount of IgG deposition (compare **a** and **b**) and 2) thickening of the glomerular membrane and deposition of C3 in membrane area (compare **c** and **d**) in *Nrf2*$^{-/-}$ but not *Nrf2*$^{+/+}$ mice. Bars are shown in microns.

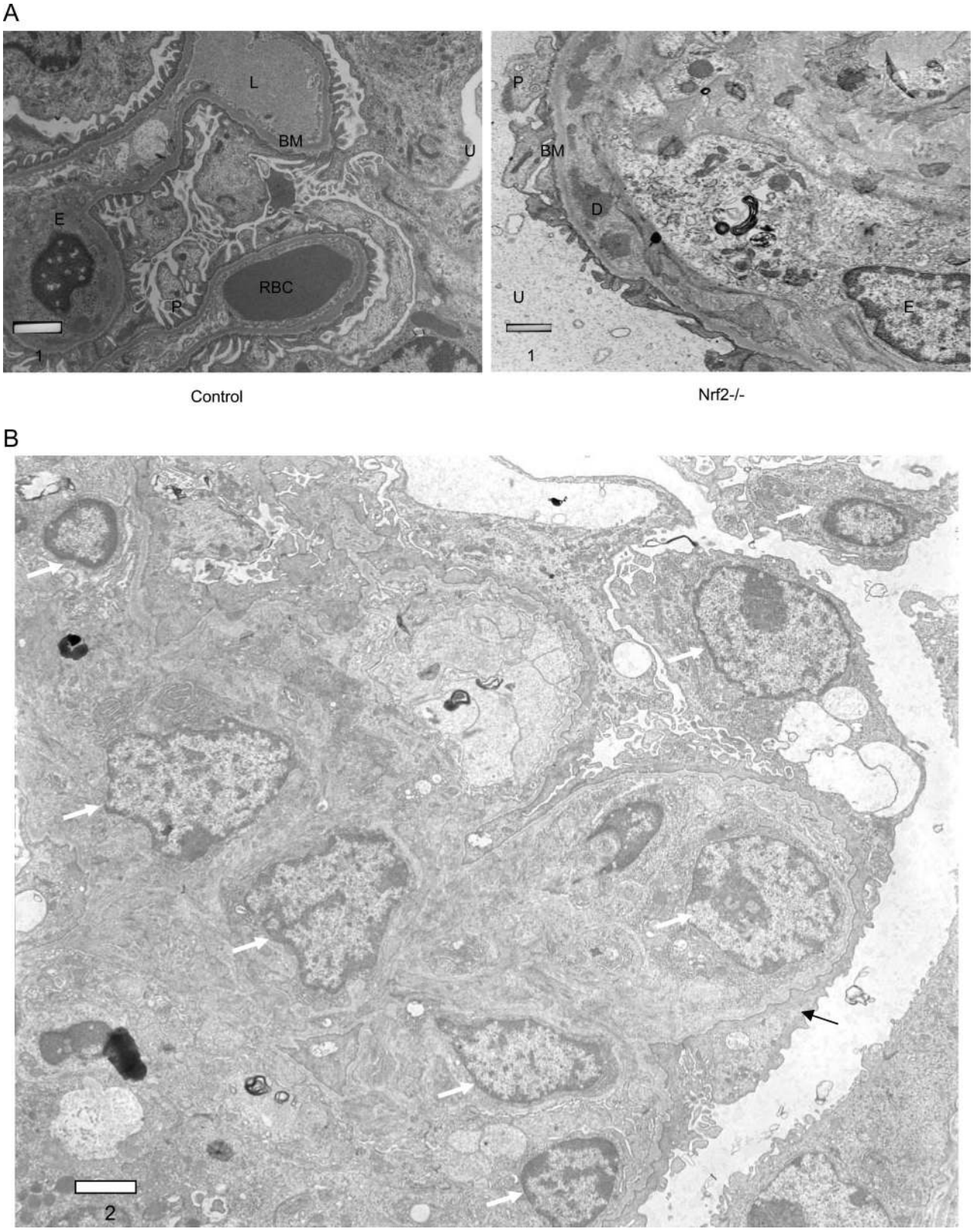

Figure 6. Electron microscopy of glomeruli. **A:** Sections from *Nrf2*$^{+/+}$ (**left**) and *Nrf2*$^{-/-}$ (**right**) mice showing thickening of basement membrane and intramembranous deposition of dense material on basement membrane in *Nrf2*$^{-/-}$ mice. D, dense deposit; BM, basement membrane; U, urinary space; P, podocyte; E, endothelial cell; RBC, red blood cell; L, capillary lumen. **B:** *Nrf2*$^{-/-}$ kidney section showing increased cellularity (**white arrow**) and effacement of podocyte foot processes (**black arrow**). Bars are in microns.

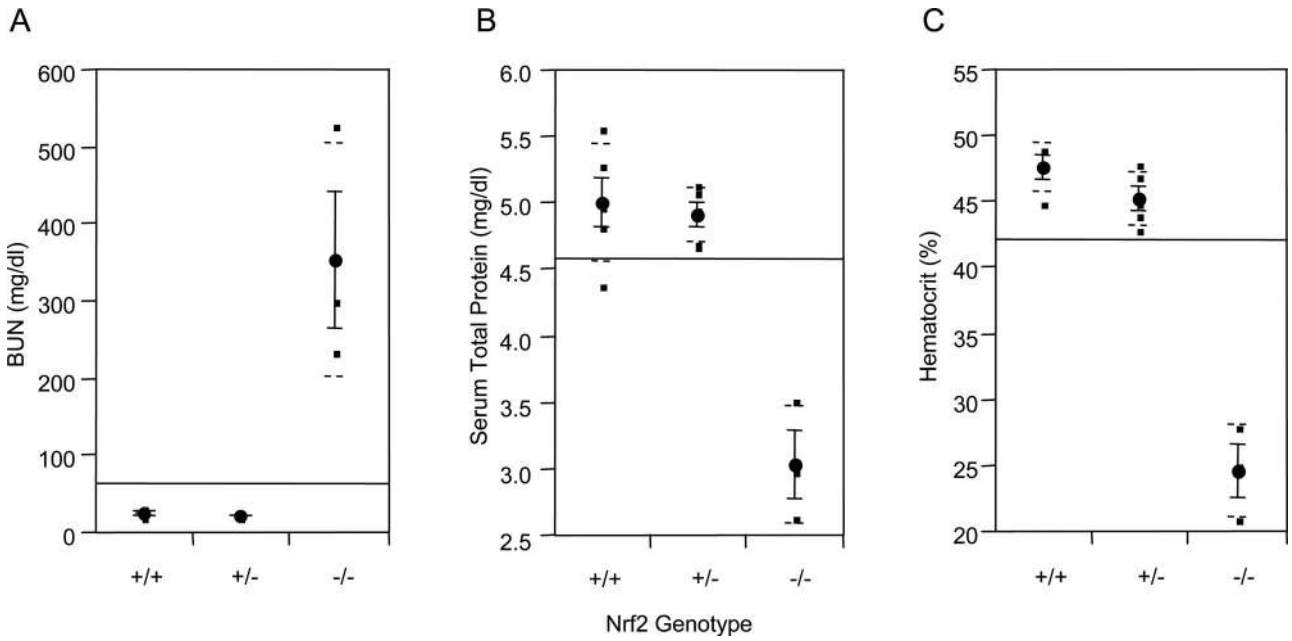

Figure 7. BUN, serum total protein, and hematocrit. Blood was taken from abdominal vena cava of *Nrf2*$^{-/-}$ mice with subcutaneous edema and age-matched control mice (*Nrf2*$^{+/-}$ and *Nrf2*$^{+/-}$). BUN (**A**), serum total protein (**B**), and hematocrit (**C**) were measured. Means and SD from four to five mice in each group were calculated with one-way analysis of variance and Tukey's multiple comparison. Genotypes are indicated on the *x* axis.

increased in *Nrf2*$^{-/-}$ mice in comparison with the controls (Figure 5, compare c and d), indicating immune complex-mediated inflammatory responses in glomerulomembranes. Electron microscopic examination of kidney sections revealed predominantly proliferative changes with expansion of mesangial matrix and deposition of dense or amorphous material in diverse glomerular locations, including intramembranous, subendothelial, and mesangial sites (Figure 6, A and B). Loss (or fusion) of foot processes of podocytes was apparent in these kidneys. Together, the findings suggest increased deposition of immunoglobulins, complement activation in glomerular basement membranes, and proliferation of mesangial cells as contributing to membranoproliferative glomerulonephritis in *Nrf2*$^{-/-}$ mice.

Serological examination showed that mice with glomerulonephritis exhibited significantly increased BUN content, decreased serum total protein level, and reduced hematocrit in comparison with age-matched wild-type and heterozygous control mice (Figure 7, A–C), which were indicative of renal failure and anemia resulting from severe glomerulonephritis.

Inflammatory Lesions in Extra-Renal Tissues of Nrf2-Null Mice

Initial necropsies of *Nrf2*$^{-/-}$ mice included histopathological examination of all tissues with gross lesions and unaffected major organs. As these necropsies were completed, an expanded spectrum of tissue changes became apparent in several mice, and additional tissues were sampled in subsequent necropsies, including all tissues with lesions and kidney, left lung lobe, heart, skin, spleen, thymus, pancreas, liver, bladder, inguinal lymph node, ileum, and mandibular salivary gland. In addition to glomerulonephritis, *Nrf2*$^{-/-}$ mice developed inflammatory lesions in multiple tissues, including lymphocytic sialitis (5 of 13 or 38%), dermatitis, hyperkeratosis, and/or epidermal clefting on the skin of the tail (which sometimes progressed to tail necrosis), myocarditis (8 of 31 or 26%), vasculitis (4 of 32 or 12%), and pancreatitis (4 of 18 or 22%). Two of the pancreatitis cases were lymphocytic pancreatitis, whereas two other cases were considered secondary to chronic-active vasculitis (one case of chronic-active, necrotizing pancreatitis and one case of proliferative pancreatitis associated with lymphoplasmacytic vasculitis with luminal obliteration and fibrinoid necrosis of vessel walls). Pleuritis and pericarditis were also frequently observed but may have been attributable to the development of thoracic transudates in mice with hypoproteinemia due to protein loss through the damaged glomeruli. Lymphocytic infiltrates were not seen in the central nervous system nor were neurological abnormalities the cause of death in any of these mice (these are the subject of a separate report currently in preparation).

As shown in Figure 8A, the salivary glands of Nrf2-null mice showed intense periductal lymphocyte infiltration, reminiscent of Sjogren's syndrome, an autoimmune disease of salivary glands often associated with systemic lupus erythematosus (SLE) in humans. Although lymphocytic infiltrates are not uncommon in mice, the 38% prevalence of lymphocytic sialitis seen in Nrf2-null mice is remarkable. In Figure 8B, myocardial vacuolar degeneration and fibrosis are demonstrated. Ocular necropsies were not routinely conducted on mice in this study. However, an occular necropsy of a representative Nrf2-null

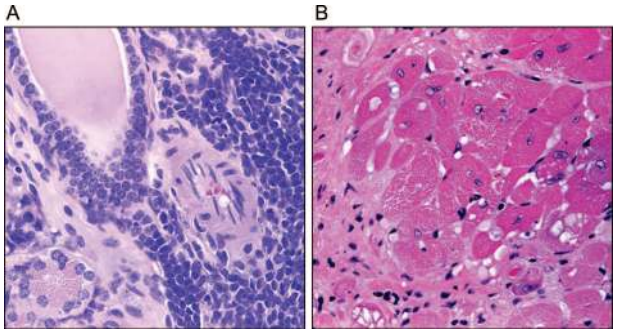

Figure 8. Lymphocytic sialitis and myocarditis. **A:** Salivary gland section from a Nrf2-null mouse was stained with H&E showing dense periductal lymphocyte infiltration composed of small and large lymphocytes and plasma cells. **B:** Left ventricle from *Nrf2*$^{-/-}$ genotype was sectioned and stained with H&E. Myocardial vacuolar degeneration and fibrosis are shown.

mouse with the occular discharge common in this strain demonstrated conjunctivitis, which varied from suppurative and lymphocytic conjunctivitis in the lower eyelids to upper eyelid alterations, which were lymphogranulomatous to pyogranulomatous with intralesional spaces consistent with lipoid material and rupture of meibomian gland contents. Associated changes included minimal to mild lymphocytic adenititis of the left and right lacrimal gland and the left harderian gland.

To further investigate the dermatitis observed in the tails of Nrf2-null mice and to distinguish primary skin changes in the tails of Nrf2-null mice from changes associated with other manifestations of immune-mediated disease, the thickened and roughened tails of one male and four female Nrf2-null mice were biopsied and compared with biopsies from four wild-type mice (two males and two females). No significant findings were observed in the wild-type mice, whereas changes were present in all Nrf2 mice, including acanthosis in four mice; four mice with additional lesions, including suppurative dermatitis, hyperkeratosis, and subcorneal and intracorneal pustules; and one mouse with suppurative and necrohemorrhagic dermatitis and myositis (Figure 9, a and c compared with b and d). Low levels of immunoglobulin deposition in the epidermis of damaged skin were observed (Figure 9, e and f).

Neoplasia was the primary cause of death in 19% (6 of 32) of mice besides glomerulonephritis. In addition, one mouse died of bacterial endocarditis and sepsis, one mouse died of hepatic infarction with necrosis, and the cause of death was undetermined in two mice. Two of the neoplasms were hemangiosarcomas based on both morphology and immunohistochemical staining for Factor 8-related antigen. On morphological grounds, three of the tumors were histiocytic proliferative disease compatible with histiocytic sarcoma, and one was lymphoproliferative disease. All mice that died or were euthanized as a result of tumors were male,

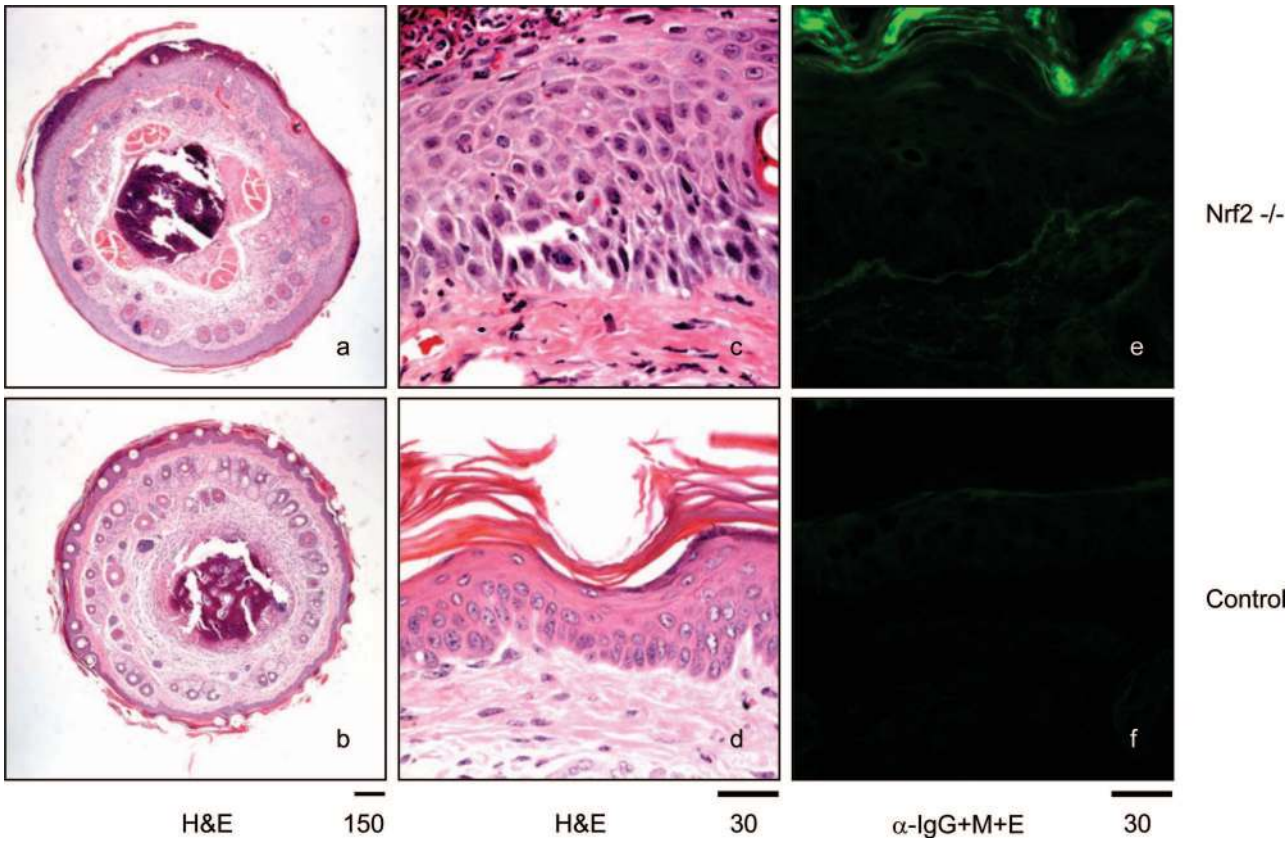

Figure 9. Skin and tail lesions. Sections of tails from control and Nrf2-null mice were stained with H&E (**a**, **b**, **c**, and **d**) or anti-immunoglobulin antibodies (**e** and **f**, α-IgG+M+E). Nrf2-null mice exhibited thickening of epidermis with acanthosis and hyperkeratosis, suppurative dermatitis on the surface of epidermis, and formation of subcorneal and intracorneal pustules (**a** and **c** compared with **b** and **d**). Immunofluorescent microscopy revealed low-level deposition of immunoglobulins in the epidermis layer of some Nrf2-null mice (compare **e** and **f**). Bars are shown in microns.

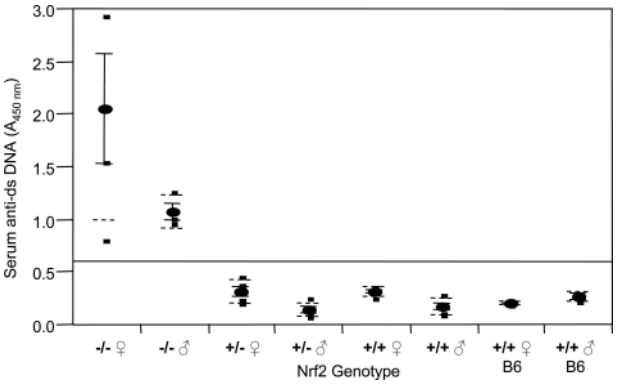

Figure 10. Serum anti-dsDNA antibody titer. Blood was collected from tail vein of age-matched *Nrf2*$^{-/-}$, *Nrf2*$^{+/-}$, and *Nrf2*$^{+/+}$ mice and C57BL/6 mice. Serum anti-dsDNA titer was determined using mouse anti-dsDNA ELISA. Means ± SD were calculated ($n = 4$ for each genotype). Statistical analysis was performed using one-way analysis of variance and Tukey's multiple comparison.

and the mean age at death was 9 ± 2 (SE) months of age.

The broad range of multitissue inflammatory lesions, along with glomerulonephritis and immunoglobulin deposition in blood vessels observed in *Nrf2*$^{-/-}$ mice, resembles the pathological characteristics of systemic lupus erythematosus (lupus) in humans, thus suggesting a role for Nrf2 in preventing the development of the autoimmune disease.

Spontaneous Development of Autoantibodies and Increased T-Cell Proliferation

A hallmark of lupus is the appearance of anti-dsDNA autoantibodies in blood. *Nrf2*$^{-/-}$ and age-matched control mice were examined for anti-dsDNA antibodies using ELISA. Serum anti-dsDNA antibodies were significantly elevated in *Nrf2*$^{-/-}$ mice in comparison with those of the homozygous and heterozygous control mice with the same 129SVJ background as well as C57BL/6 mice (Figure 10) ($P < 0.0001$). The means of anti-dsDNA in *Nrf2*$^{-/-}$ mice were in the range of 1.0 to 2.1, whereas those of the control mice were from 0.14 to 0.32. In addition, the anti-dsDNA titers in female *Nrf2*$^{-/-}$ mice were twice as high as those of male *Nrf2*$^{-/-}$ mice, which was in agreement with a higher prevalence and greater severity of the immune-mediated diseases in females than in males.

The elevation of anti-dsDNA antibody titers suggests an abnormality in autoimmune tolerance. Therefore, we analyzed the functions of T and B cells in *Nrf2*$^{-/-}$ mice. Peripheral lymphocytes were isolated from lymph nodes and the spleen, and the cells were examined for response to proliferative stimuli. Figure 11A shows that T cells from *Nrf2*$^{-/-}$ mice exhibited enhanced proliferation on stimulation with anti-CD3 (a T-cell stimulant) in comparison with controls ($P < 0.01$). To further examine which subset of T cells accounted for the proliferation, CD4$^+$ and CD8$^+$ cells were isolated. The CD4$^+$ cells from *Nrf2*$^{-/-}$ mice were shown to have increased proliferation in response to anti-CD3 ($P < 0.05$) (Figure 11B), whereas CD8$^+$ cells from *Nrf2*$^{-/-}$ and *Nrf2*$^{+/+}$ cells proliferated similarly under the same conditions (data not shown). B cells were isolated from the spleens of *Nrf2*$^{+/+}$ and *Nrf2*$^{-/-}$ mice and were examined for proliferation in response to lipopolysaccharide or anti-mouse IgM (both stimulants of B-cell proliferation). The results revealed that B cells from Nrf2 wild-type and -null mice proliferate similarly to each other in response to the B-cell stimulants (data not shown). The compositions of peripheral CD4$^+$ and CD8$^+$ cells were analyzed by FACS. CD4$^+$ and CD8$^+$ cells each accounted for 20% of lymph node cells in *Nrf2*$^{+/+}$ mice. However, in *Nrf2*$^{-/-}$ mice, the fraction of CD4$^+$ cells was increased compared with controls (30 versus 20%), whereas that of CD8$^+$ was reduced (14 versus 20%) (Figure 12). Taken together, these results suggest that loss of Nrf2 function is associated with an altered balance between peripheral CD4$^+$ and CD8$^+$

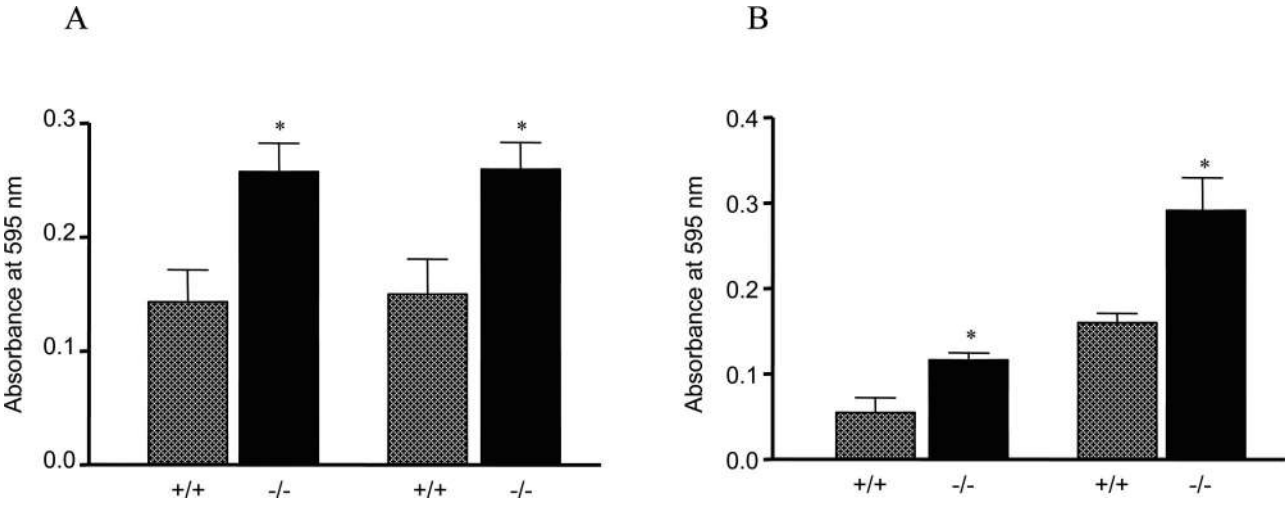

Figure 11. Lymphocyte proliferation. Peripheral lymphocytes were collected from lymph nodes (mandibular and axillary regions) from 6-month-old mice. CD4$^+$ cells were isolated using BD IMagnet. Lymph node cells (**A**) or CD4$^+$ lymphocytes (**B**) were seeded at a density of either 4×10^4 (**left**) or 1×10^5 (**right**). The cells were stimulated with anti-CD3 antibodies for 48 hours. Proliferation was measured with the MTT kit. ▨, *Nrf2*$^{+/+}$; ■, *Nrf2*$^{-/-}$. Data represent means ± SD from three samples. *$P < 0.05$.

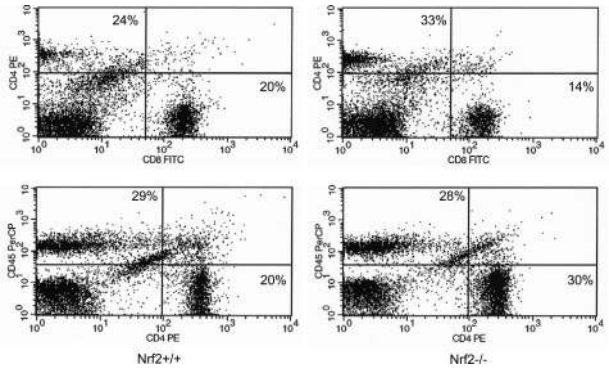

Figure 12. FACS analysis of lymph node lymphocytes. Lymphocytes were isolated from lymph nodes of Nrf2$^{+/+}$ (**left**) and Nrf2$^{-/-}$ (**right**) mice; the cells were immunostained with anti-CD4, -CD8, and -CD45R/B220 antibodies and analyzed by FACS.

lymphocytes, which contributed to the development of immune-mediated disease in the mice. Hyperproliferation of T cells may also contribute to the adenopathy and splenomegaly observed in Nrf2-null mice (Figure 2C).

Reduced Expression of Antioxidant-Inducible Genes and Increased Oxidative Lesions in Tissues of Nrf2-Null Mice

Nrf2 is activated by a range of structurally diverse antioxidants, typified by phenolic antioxidants BHA and tBHQ. In wild-type mice, BHA induces two sets of genes: 1) phase II drug-metabolizing enzymes, such as *Nqo1 and GstA1*, and 2) antioxidant genes, such as *Ho-1*. The role of Nrf2 in the transcriptional regulation of these genes remains largely to be established. The high incidence of autoimmunity and enhanced lymphocyte proliferation in Nrf2-null mice raised the possibility that certain target genes of Nrf2 play critical roles in the control of self-tolerance, ie, loss of expression/induction of the genes contributes to immune disregulation. Thus, we examined the Nrf2 dependence in the expression of a panel of BHA-inducible genes in Nrf2-null mice. Female wild-type and Nrf2-null mice were treated with BHA or corn oil. Induction of the genes was analyzed by Northern blotting. As shown in Figure 13A, phase II genes *Nqo1*, *GstA1, UDP glucuronosyltransferase A1* (*UgtA1*), and *epoxide hydrolase 1* (*Ephx1*) were constitutively expressed in the liver and were induced by BHA in wild-type mice; however, in Nrf2-null mice, induction of the genes, as well as the constitutive expression of *Nqo1* and *GstA1*, was lost. Phase II genes *Ephx2* and *N-acetyltransferase 2* were expressed similarly in both wild-type and Nrf2-null mice in the absence or presence of BHA. *Ho-1* and *glutathione synthetase-S* (*Gsh-S*) were induced by BHA in wild-type mice, but the induction was reduced or lost in *Nrf2*$^{-/-}$ mice. Thus, the Nrf2-null mice are devoid of the basal expression of *Nqo1* and *GstA1* as well as the induction of phase II genes (*Nqo1*, *GstA1, UgtA1,* and *Ephx1*) and antioxidative genes (*Ho-1* and *Gsh-S*). We further examined whether Nrf2-null function affects the regulation of the ARE-driven genes in lymphoid tissues. Total RNA from the spleens of *Nrf2*$^{+/+}$ and *Nrf2*$^{-/-}$ mice treated with

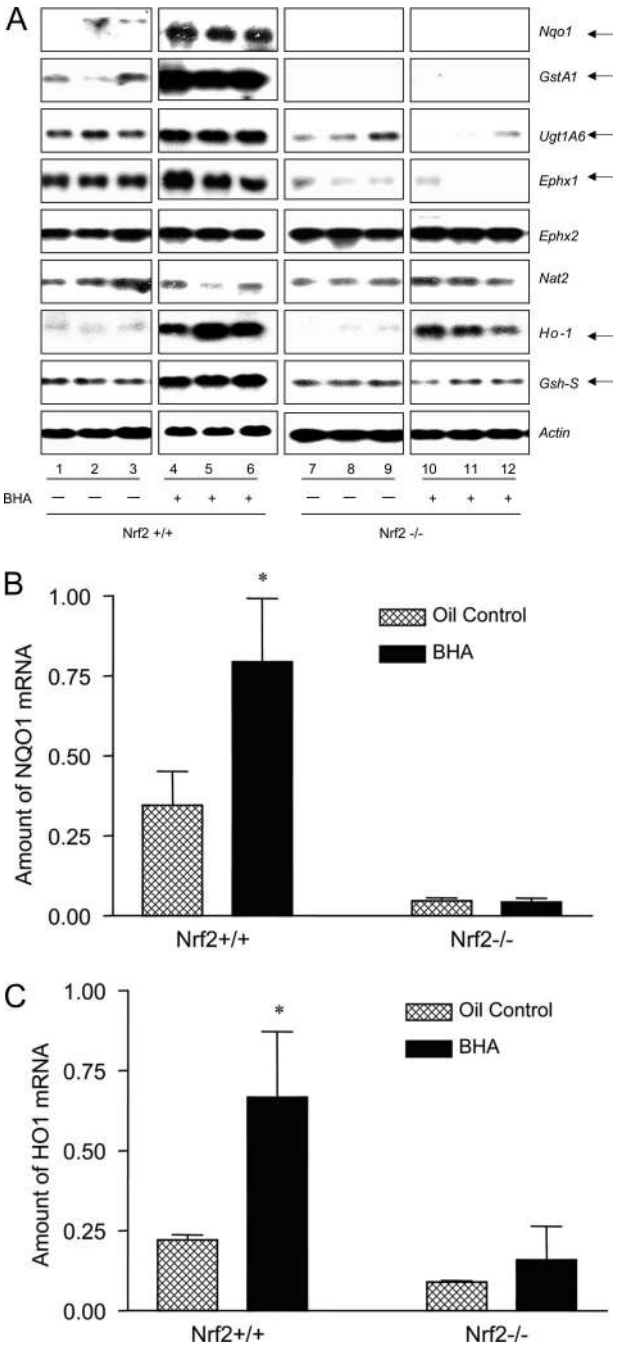

Figure 13. Regulation of phase II and antioxidant genes by Nrf2. *Nrf2*$^{+/+}$ and *Nrf2*$^{-/-}$ mice (2 months) were treated with corn oil or BHA (intragastric, treatment on days 1 and 3, 400 mg/kg body weight). Liver and spleen samples were taken out on day 4 and stored in RNALater (Qiagen). **A:** Total RNA from liver was prepared and analyzed by Northern blotting. Each group consists of three mice; each gene was analyzed with the same gel and exposure. *Actin* was used to ensure equal loading among samples. **Arrows** indicate genes with altered basal and/or inducible expressions in Nrf2-null mice. **B** and **C:** Total RNA from spleen was analyzed by real-time PCR. Data represent means ± SD from three samples. *$P < 0.05$.

BHA or corn oil was analyzed for expression of *Nqo1* and *Ho-1* by real-time PCR (Figure 13, B and C). The mRNAs of both genes were readily detected constitutively, but the levels were reduced in *Nrf2*$^{-/-}$ mice. Both were significantly induced by BHA in wild-type mice but not in null mice. Thus, Nrf2 controls the basal and inducible expres-

sion of *Nqo1* and *Ho-1* in splenocytes similarly to that in hepatocytes *in vivo*.

We examined whether lost or reduced expression and induction of detoxification and antioxidative enzymes/proteins increased oxidative tissue damage in Nrf2-null mice. Liver and kidney tissues were taken from female wild-type or Nrf2-null mice (6 months of age). Oxidative tissue damage was analyzed by measuring free MDA content, which reflects levels of lipid peroxidation. The results revealed that MDA formation was significantly increased in both the liver (Figure 14A) and the kidney (Figure 14B) of the Nrf2-null mice in comparison with those of wild-type mice ($P < 0.05$). In Figure 14C, MDA production in the liver was shown to increase age-dependently in both genotypes. At the age of 1 month, the MDA contents were slightly higher in *Nrf2*$^{-/-}$ mice than in the wild-type. The differences were significantly increased at the ages of 5.5 and 11.5 months. The results indicate that Nrf2-null mice exhibited increased oxidative tissue damage in the absence of exposure to exogenous oxidants and suggest a synergistic effect on oxidative damage between Nrf2-null function and aging.

Discussion

Examination of mice deficient in Nrf2, which functions as a sensor and transcriptional mediator to antioxidants and oxidative signals, has led to the identification of important functions of Nrf2 in self-tolerance in the absence of apparent exposure to exogenous chemicals. Notably, *Nrf2*$^{-/-}$ mice developed complex disease manifestations with features of multiorgan inflammatory infiltrates, elevated serum anti-dsDNA antibodies in young adulthood, deposition of immunoglobulin complexes in glomerular basement membrane, and premature death due to glomerulonephritis and renal failure. Moreover, Nrf2-deficient CD4^{+} T lymphocytes hyperproliferate in response to T cell receptor (TCR) stimulation. Lastly, the *Nrf2*$^{-/-}$ mice have decreased or abolished expression and induction of certain phase II and antioxidant genes and increased oxidative lesions in tissues. Thus, a potential mechanism for Nrf2-mediated regulation of autoimmune function involves Nrf2 suppressing oxidative tissue damage and T-cell proliferation.

Several characteristics of the autoimmune-mediated lesions observed in the *Nrf2*$^{-/-}$ mice were similar to those of the human systemic lupus erythematosus. These include 1) erythematous skin lesions, membranoproliferative glomerulonephritis, serosities, and lymphocytic sialitis; 2) high levels of anti-dsDNA antibodies with renal deposition of immune complexes; 3) female predominance; and 4) variable courses of development. Interestingly, Yoh et al reported increased incidence of immune-mediated nephritis in a separate strain (ICR) of Nrf2-deficient mice.[22] The immune-mediated glomerulonephritis in the ICR strain was also predominantly observed in females but at an older age (>60 weeks of age). The cause of the apparent age difference of the immune-mediated glomerulonephritis in Nrf2-deficient mice between the report by Yoh et al and our report is not known at present but may be attributable to differences in the genetic backgrounds of the two strains (ie, ICR versus 129SVJ). Nonetheless, the studies concur that loss of Nrf2 function predisposed mice to the development of lupus-like, systemic immune-mediated disease, principally characterized by membranoproliferative glomerulonephritis. Also consistent with SLE in humans, IgG, IgM, IgA, and C3 were all found in glomerular capillary deposits. Interestingly, dense deposits were predominantly intramembranous in *Nrf2*$^{-/-}$ mice. In addition, subendo-

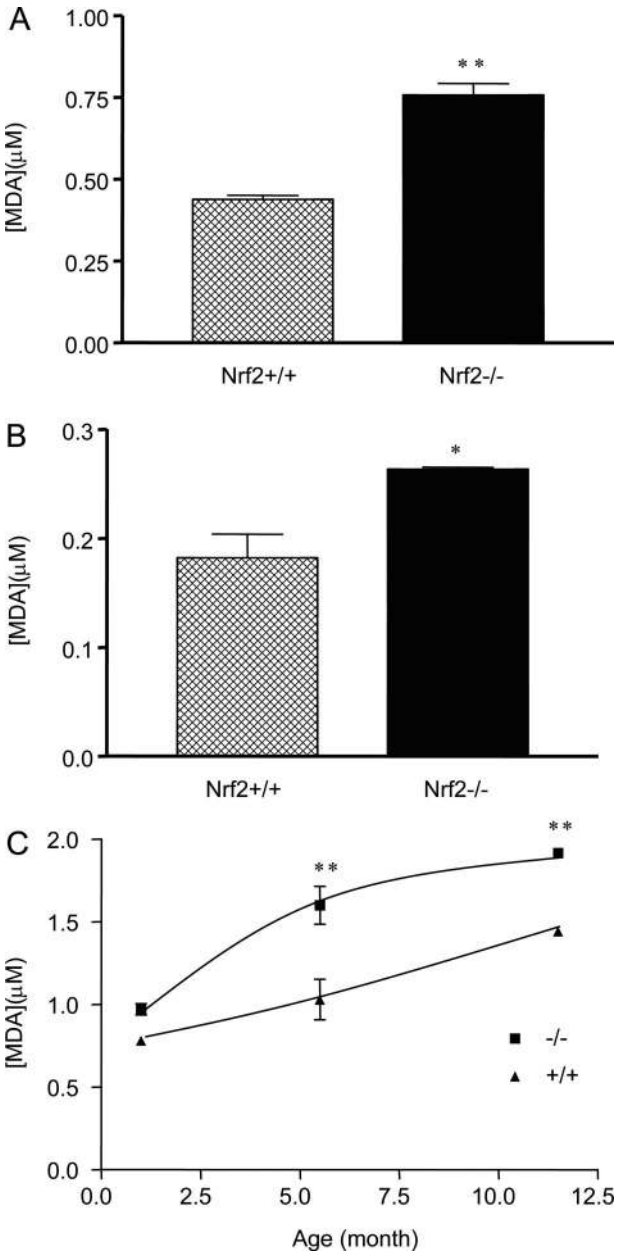

Figure 14. Lipid peroxidation. Liver (**A**) and kidney (**B**) were taken from *Nrf2*$^{+/+}$ and *Nrf2*$^{-/-}$ mice (female, 6 months old). Homogenates were prepared and measured for free MDA using the Bioxytech MDA-586 kit. **C:** Liver samples were taken from age-matched female *Nrf2*$^{+/+}$ and *Nrf2*$^{-/-}$ mice. MDA in tissue homogenates was measured. Data represent means ± SD from three mice in each group. Statistical analysis was performed using GraphPad PRISM software (GraphPad Software, Inc., San Diego, CA). *$P < 0.05$; **$P < 0.01$.

thelial and intramembranous deposits of amorphous material with varying electron density were observed in the glomeruli of *Nrf2*$^{-/-}$ mice. The most consistent light and electron microscopic finding in the glomeruli of *Nrf2*$^{-/-}$ mice was proliferation, predominantly of mesangial cells. In contrast to the previous report of glomerulonephritis,[22] electron-dense deposits were not common in wild-type mice and, in fact, were seen in only one mouse in this series. Thus, our finding suggests that the absence of Nrf2 plays a role in the initiation of autoimmune disease rather than in its progression. As in human SLE, mesangial proliferation is a prominent feature of glomerulonephritis in these mice.

The development of SLE involves polyclonal activation of T and B lymphocytes, production of autoantibodies against nuclear and cytoplasmic macromolecules, and deposition of immune complexes in tissues, followed by a cascade(s) of inflammatory responses resulting in tissue damage.[23,24] Evidence reveals that a complex interlay of genetic, environmental, and hormonal factors modulates these pathogenic mechanisms and thereby determine the manifestation, severity, and course of the disease.[24,25] In particular, analyses of several experimental mouse models with spontaneous lupus-like syndromes have led to the identification of a number of candidate susceptibility genes of SLE, including class II major histocompatibility complex, complements, and immunoglobulin γ receptors IIa and IIIa. Furthermore, targeted disruption of certain genes or creation of transgenic strains with aberrant/overexpression of immune regulatory pathways have generated a collection of models of autoimmunity resembling SLE. Analyses of the models have not only revealed a large number of regulatory factors of SLE but also provided mechanistic insights into the effector mechanism involved in disease pathogenesis, the genetic mechanism leading to systemic autoimmunity, and the genetic interactions among susceptibility factors. It is noteworthy that enhanced proliferation of lymphocytes and elevated production of autoantibodies are common components of the systemic autoimmune syndromes observed in these mouse models. In our analysis of lymphocyte functions of *Nrf2*$^{-/-}$ mice, we found that peripheral CD4$^+$ but not CD8$^+$ T cells showed significantly enhanced proliferative response to anti-CD3 antibodies, a T-cell stimulant, giving rise to an increased ratio of CD4$^+$ to CD8$^+$ cells. On the other hand, B cells from *Nrf2*$^{-/-}$ spleens proliferate similarly to *Nrf2*$^{+/+}$ cells on exposure to B-cell stimulants. It is known that the loss of anergy of anti-dsDNA B cells requires both the production of T helper cells and the overcoming of T suppressor cells.[26] Therefore, our results implicate CD4$^+$ hyperproliferation in the development of autoimmunity in *Nrf2*$^{-/-}$ mice. Nrf2 may negatively control CD4$^+$ T-cell proliferation by inhibiting cell growth. Alternatively, Nrf2 regulates the sensitivity of CD4$^+$ cells to growth stimulants by modulating the threshold of CD4$^+$ cells to growth stimulants.

Analysis of a panel of phase II and antioxidant genes that are potentially regulated by AREs in *Nrf2*$^{-/-}$ females confirmed that Nrf2 is required for the induction of a number of ARE-regulated genes by antioxidants in both hepatic and lymphoid tissues (Figure 13). Ablation of Nrf2 reduces or abolishes the induction of phase II genes *Nqo1*, *GstA1*, *UgtA1*, and *Ephx1* and antioxidant genes *Ho-1* and *Gsh-S*, as well as the basal expression of *Nqo1* and *GstA1*. It is known that these genes are directly or indirectly involved in the homeostasis of ROS. Reduction or loss of the expression and induction of the genes would result in increased oxidative stress in tissues. Increased lipid peroxidation (as indicated by elevated free MDA levels) is observed in the kidney, liver, and other tissues of *Nrf2*$^{-/-}$ mice. Furthermore, our data revealed a synergy between Nrf2-null function and aging on MDA production *in vivo* (Figure 14). This notion is supported by other reports in which real-time electron paramagnetic resonance imaging and spin probe kinetic analysis were used to examine the tissue-reducing activity of *Nrf2*$^{-/-}$ mice; the results indicated that Nrf2 deficiency plus aging significantly reduces the reducing capability in certain tissues of ICR mice.[27] Together, these data provide direct evidence supporting a critical role of Nrf2 in the control of ROS homeostasis in intact animals.

Three lines of observation implicate oxidative stress in the loss of self-tolerance. First, exposure of lymphocytes to ROS, in particular H_2O_2, can mimic the effect of antigen exposure, leading to lymphocyte activation and proliferation. Moreover, antigen receptors are themselves H_2O_2-generating enzymes, raising the possibility of H_2O_2 as a second messenger in lymphocyte activation.[28] Second, targeted knockout or certain polymorphisms of antioxidant genes, including target genes of Nrf2, were associated with immune-mediated nephritis.[29,30] Third, supplementation of ω-3 fatty acids (as an antioxidant) up-regulated the expression of antioxidant enzymes (catalase, glutathione peroxidase, and superoxide dismutase) and delayed the onset and progression of autoimmune nephritis, thereby extending the life-span of lupus-prone NZB/NZW F1 female mice significantly.[31] The correlation of impaired ROS homeostasis and autoimmune dysfunction observed in Nrf2-null mice supports a role of oxidative stress in lupus-like autoimmune regulation. It is known that loss of Nrf2 results in increased apoptosis due to increased ROS.[16,32] Moreover, phagocytosis and clearance of apoptotic cells by macrophages have been linked to exposure of autoantigens to immune cells in the production of autoantibodies.[33] Thus, our results provide a straightforward model to explain the breakdown in peripheral tolerance in *Nrf2*$^{-/-}$ mice: loss of Nrf2 causes oxidative tissue damage and apoptosis, which increase the production and exposure of autoantigens to immune cells, resulting in the activation of CD4$^+$ cells and production of autoantibodies by B cells, leading to systemic autoimmune damage.

An alternative explanation of the autoimmune dysfunction in *Nrf2*$^{-/-}$ mice derives from the observation that the loss of function of certain drug-metabolizing enzymes (by targeted knockout or due to certain polymorphic genotypes) is associated with increased autoimmunity.[30,34,35] In this scenario, altered metabolism of an endogenous or dietary chemical(s) in *Nrf2*$^{-/-}$ animals due to decreased expression of phase II enzymes may lead to increased production of reactive intermediates (other than ROS)

that form haptens or directly damage macromolecules and cellular structures, both of which increase autoantigen production and activation of immune cells causing autoimmune response to self-tissues.

A prominent feature of lupus-like autoimmune syndromes is that many of the disorders can be induced or precipitated by drugs, pesticides, cosmetics, heavy metals, and other environmental, dietary, and occupational chemicals, thus underlining the importance of gene-environment interaction in autoimmune pathogenesis.[36–40] Although it is unclear at present whether Nrf2 and its downstream enzymes are involved in chemical-induced autoimmune disorders, the critical role of Nrf2-regulated enzymes in the detoxification of a wide range of chemicals and the high inducibility of the enzymes by a variety of chemicals with diverse structures support such a role of Nrf2. In this regard, the Nrf2-null mice may provide a model system for analyzing possible interplay among lupus-inducing chemicals, drug metabolism, ROS generation, autoantibody production, and downstream pathogenic mechanisms in drug/toxicant-induced autoimmune dysfunctions in future.

Acknowledgments

We thank Drs. R. Mercer and J. Ma for National Institute for Occupational Safety and Health internal review of the manuscript; S. Friend for the preparation of ultrastructural specimens; D. Newcomer and P.A. Willard for preparing light microscopy sections; M.G. Chen for real-time PCR; and Dr. P. Nicolaysen for insightful suggestions on animal caretaking.

References

1. Mohler J, Vani K, Leung S, Epstein A: Segmentally restricted, cephalic expression of a leucine zipper gene during Drosophila embryogenesis. Mech Dev 1991, 34:3–9
2. Chan JY, Cheung MC, Moi P, Chan K, Kan YW: Chromosomal localization of the human NF-E2 family of bZIP transcription factors by fluorescence in situ hybridization. Hum Genet 1995, 95:265–269
3. Chan JY, Han XL, Kan YW: Isolation of cDNA encoding the human NF-E2 protein. Proc Natl Acad Sci USA 1993, 90:11366–11370
4. Andrews NC, Erdjument-Bromage H, Davidson MB, Tempst P, Orkin SH: Erythroid transcription factor NF-E2 is a haematopoietic-specific basic-leucine zipper protein. Nature 1993, 362:722–728
5. Chan JY, Han XL, Kan YW: Cloning of Nrf1, an NF-E2-related transcription factor, by genetic selection in yeast. Proc Natl Acad Sci USA 1993, 90:11371–11375
6. Moi P, Chan K, Asunis I, Cao A, Kan YW: Isolation of NF-E2-related factor 2 (Nrf2), a NF-E2-like basic leucine zipper transcriptional activator that binds to the tandem NF-E2/AP1 repeat of the beta-globin locus control region. Proc Natl Acad Sci USA 1994, 91:9926–9930
7. Itoh K, Igarashi K, Hayashi N, Nishizawa M, Yamamoto M: Cloning and characterization of a novel erythroid cell-derived CNC family transcription factor heterodimerizing with the small Maf family proteins. Mol Cell Biol 1995, 15:4184–4193
8. Oyake T, Itoh K, Motohashi H, Hayashi N, Hoshino H, Nishizawa M, Yamamoto M, Igarashi K: Bach proteins belong to a novel family of BTB-basic leucine zipper transcription factors that interact with MafK and regulate transcription through the NF-E2 site. Mol Cell Biol 1996, 16:6083–6095
9. Chan K, Lu R, Chang JC, Kan YW: NRF2, a member of the NRE2 family of transcription factors, is not essential for murine erythropoiesis, growth, and development. Proc Natl Acad Sci USA 1996, 93:13943–13948
10. Ramos-Gomez M, Kwak MK, Dolan PM, Itoh K, Yamamoto M, Talalay P, Kensler TW: Sensitivity to carcinogenesis is increased and chemoprotective efficacy of enzyme inducers is lost in nrf2 transcription factor-deficient mice. Proc Natl Acad Sci USA 2001, 98:3410–3415
11. Chan K, Han XD, Kan YW: An important function of Nrf2 in combating oxidative stress: detoxification of acetaminophen. Proc Natl Acad Sci USA 2001, 98:4611–4616
12. Cho HY, Jedlicka AE, Reddy SP, Kensler TW, Yamamoto M, Zhang LY, Kleeberger SR: Role of NRF2 in protection against hyperoxic lung injury in mice. Am J Respir Cell Mol Biol 2002, 26:175–182
13. Chan K, Kan YW: Nrf2 is essential for protection against acute pulmonary injury in mice. Proc Natl Acad Sci USA 1999, 96:12731–12736
14. Li N, Alam J, Venkatesan MI, Eiguren-Fernandez A, Schmitz D, Di Stefano E, Slaughter N, Killeen E, Wang X, Huang A, Wang M, Miguel AH, Cho A, Sioutas C, Nel AE: Nrf2 is a key transcription factor that regulates antioxidant defense in macrophages and epithelial cells: protecting against the proinflammatory and oxidizing effects of diesel exhaust chemicals. J Immunol 2004, 173:3467–3481
15. Hu X, Roberts JR, Apopa PL, Kan YW, Ma Q: Accelerated ovarian failure induced by 4-vinyl cyclohexene diepoxide in Nrf2 null mice. Mol Cell Biol 2006, 26:940–954
16. Leung L, Kwong M, Hou S, Lee C, Chan JY: Deficiency of the Nrf1 and Nrf2 transcription factors results in early embryonic lethality and severe oxidative stress. J Biol Chem 2003, 278:48021–48029
17. Nguyen T, Sherratt PJ, Pickett CB: Regulatory mechanisms controlling gene expression mediated by the antioxidant response element. Annu Rev Pharmacol Toxicol 2003, 43:233–260
18. Ma Q, Kinneer K, Bi Y, Chan JY, Kan YW: Induction of murine NAD(P)H:quinone oxidoreductase by 2,3,7,8-tetrachlorodibenzo-p-dioxin requires the CNC (cap 'n' collar) basic leucine zipper transcription factor Nrf2 (nuclear factor erythroid 2-related factor 2): cross-interaction between AhR (aryl hydrocarbon receptor) and Nrf2 signal transduction. Biochem J 2004, 377:205–213
19. He CH, Gong P, Hu B, Stewart D, Choi ME, Choi AM, Alam J: Identification of activating transcription factor 4 (ATF4) as an Nrf2-interacting protein: implication for heme oxygenase-1 gene regulation. J Biol Chem 2001, 276:20858–20865
20. Kim YC, Masutani H, Yamaguchi Y, Itoh K, Yamamoto M, Yodoi J: Hemin-induced activation of the thioredoxin gene by Nrf2: a differential regulation of the antioxidant responsive element by a switch of its binding factors. J Biol Chem 2001, 276:18399–18406
21. Ma Q, Renzelli AJ, Baldwin KT, Antonini JM: Superinduction of CYP1A1 gene expression: regulation of 2,3,7,8-tetrachlorodibenzo-p-dioxin-induced degradation of Ah receptor by cycloheximide. J Biol Chem 2000, 275:12676–12683
22. Yoh K, Itoh K, Enomoto A, Hirayama A, Yamaguchi N, Kobayashi M, Morito N, Koyama A, Yamamoto M, Takahashi S: Nrf2-deficient female mice develop lupus-like autoimmune nephritis. Kidney Int 2001, 60:1343–1353
23. Marshall E: Lupus: mysterious disease holds its secrets tight. Science 2002, 296:689–691
24. Wakeland EK, Liu K, Graham RR, Behrens TW: Delineating the genetic basis of systemic lupus erythematosus. Immunity 2001, 15:397–408
25. Vyse TJ, Kotzin BL: Genetic susceptibility to systemic lupus erythematosus. Annu Rev Immunol 1998, 16:261–292
26. Seo SJ, Fields ML, Buckler JL, Reed AJ, Mandik-Nayak L, Nish SA, Noelle RJ, Turka LA, Finkelman FD, Caton AJ, Erikson J: The impact of T helper and T regulatory cells on the regulation of anti-double-stranded DNA B cells. Immunity 2002, 16:535–546
27. Hirayama A, Yoh K, Nagase S, Ueda A, Itoh K, Morito N, Hirayama K, Takahashi S, Yamamoto M, Koyama A: EPR imaging of reducing activity in Nrf2 transcriptional factor-deficient mice. Free Radic Biol Med 2003, 34:1236–1242
28. Flemming A, Brummer T, Reth M, Jumaa H: The adaptor protein SLP-65 acts as a tumor suppressor that limits pre-B cell expansion. Nat Immunol 2003, 4:38–43
29. Poss KD, Tonegawa S: Heme oxygenase 1 is required for mammalian iron reutilization. Proc Natl Acad Sci USA 1997, 94:10919–10924
30. Fraser PA, Ding WZ, Mohseni M, Treadwell EL, Dooley MA, St Clair EW, Gilkeson GS, Cooper GS: Glutathione S-transferase M null ho-

mozygosity and risk of systemic lupus erythematosus associated with sun exposure: a possible gene-environment interaction for autoimmunity. J Rheumatol 2003, 30:276–282
31. Chandrasekar B, Fernandes G: Decreased pro-inflammatory cytokines and increased antioxidant enzyme gene expression by omega-3 lipids in murine lupus nephritis. Biochem Biophys Res Commun 1994, 200:893–898
32. Morito N, Yoh K, Itoh K, Hirayama A, Koyama A, Yamamoto M, Takahashi S: Nrf2 regulates the sensitivity of death receptor signals by affecting intracellular glutathione levels. Oncogene 2003, 22:9275–9281
33. Scott RS, McMahon EJ, Pop SM, Reap EA, Caricchio R, Cohen PL, Earp HS, Matsushima GK: Phagocytosis and clearance of apoptotic cells is mediated by MER. Nature 2001, 411:207–211
34. Ward JM, Nikolov NP, Tschetter JR, Kopp JB, Gonzalez FJ, Kimura S, Siegel RM: Progressive glomerulonephritis and histiocytic sarcoma associated with macrophage functional defects in CYP1B1-deficient mice. Toxicol Pathol 2004, 32:710–718
35. McKinnon RA, Nebert DW: Possible role of cytochromes P450 in lupus erythematosus and related disorders. Lupus 1994, 3:473–478
36. Rowley B, Monestier M: Mechanisms of heavy metal-induced autoimmunity. Mol Immunol 2005, 42:833–838
37. D'Cruz D: Autoimmune diseases associated with drugs, chemicals and environmental factors. Toxicol Lett 2000, 112–113:421–432
38. Pieters R, Ezendam J, Nierkens S: Chemical-specific properties codetermine the type of adverse immune response. Autoimmun Rev 2003, 2:25–29
39. Holsapple MP: Autoimmunity by pesticides: a critical review of the state of the science. Toxicol Lett 2002, 127:101–109
40. Martin SF: T lymphocyte-mediated immune responses to chemical haptens and metal ions: implications for allergic and autoimmune disease. Int Arch Allergy Immunol 2004, 134:186–198